AIAA JOURNAL
Vol. 34, No. 1, January 1996

Efficient Modeling of Postbuckling Delamination Growth in Composite Laminates Using Plate Elements

J. Klug,* X. X. Wu,† and C. T. Sun‡
Purdue University, West Lafayette, Indiana 47907-1282

Under compression, delaminated composite plates may undergo postbuckling that can lead to delamination growth. The use of three-dimensional finite elements for the calculation of the strain energy release rate at the delamination front is computationally expensive. The Mindlin plate finite element is used to perform the postbuckling analysis and to compute the strain energy release rate at the delamination front with the aid of the crack closure method. Comparison of the present strain energy release rate calculation with the existing three-dimensional result indicates that the present method is efficient and accurate. For stationary delamination cracks, the effects of stacking sequence and shape of delamination are examined. A procedure of determining delamination front location for a propagating delamination is presented. Delamination growth initiated from embedded and edge delaminations is investigated using this procedure.

Nomenclature

$[A]$, $[B]$, $[D]$	= classical laminated plate theory extension, bending-extension, and bending stiffness matrices, respectively
a	= ellipse axis length in x direction
b	= ellipse axis length in y direction
G	= total strain energy release rate
G_{cr}	= critical value of the strain energy release rate
h_1	= thickness of upper sublaminate
h_2	= thickness of lower sublaminate
M_x, M_y	= reaction nodal moments
N_x, N_y, N_z	= reaction nodal forces
r	= ellipse aspect ratio defined as b/a
s	= arc length of delamination front
u_x^0, u_y^0, u_z^0	= plate midplane displacements in the respective directions
W	= overall plate length in y direction for edge delamination
$2L$	= overall plate length in x direction
$2W$	= overall plate length in y direction for embedded delamination
Δa	= delamination front crack length
ε_0	= applied strain loading level
ψ_x, ψ_y	= rotations of the cross sections perpendicular to the x and y axes, respectively

I. Introduction

DAMAGE can arise from the forced fitting of composite parts during the assembly of a structure or from impact by foreign objects during service. The most dominant form of damage is delamination due to lack of reinforcement in the thickness direction. Delamination may cause a significant reduction in the load-carrying capacity of laminated composite structures. A good understanding of delamination growth is essential to damage tolerance design.

Under compression, the delaminated part of the composite plate may undergo postbuckling. Numerous analytical and numerical studies have been performed on this subject. These studies began with the analysis of a one-dimensional or through-the-width delamination.[1-3] Chai et al.[1] were perhaps the first to characterize the delamination buckling models by the delamination thickness and number of delaminations through the laminate thickness. Strain energy release rate was calculated by differentiating the strain energy with respect to the delamination and growth distance. Use of the crack closure technique was initiated by Whitcomb,[2] who analyzed the effects of various parameters on the strain energy release rate in a beamlike structure using geometrically nonlinear finite elements.

Much research on embedded delamination has been performed using the Rayleigh–Ritz method.[4-8] In these analyses a polynomial form of the transverse displacement field was adopted. Yin and Jane[4,5] determined the order of the polynomial form necessary to accurately compute the bifurcation load, deflection, force and moment resultants, and strain energy release rate. Delamination growth was achieved by lengthening the respective ellipse axis where the critical value of the strain energy release rate was exceeded.

Whitcomb[9-13] used the virtual crack closure technique in conjunction with the three-dimensional or plate finite element analysis to study various delamination problems. In his work, out-of-plane displacement in the midplane of the laminate was constrained in order to remove the effects of global buckling. The effect of contact of the delamination crack surfaces was considered. Whitcomb[9] concluded that for some cases it might be possible to overlook the effect of contact or overlapping of sublaminates in the delamination zone.

The growth of a circular delamination for isotropic plates and cross-ply laminates has been studied by Nilsson and Giannakopoulos[14] and Nilsson et al.[15] using plate finite elements. In their analyses, the out-of-plane displacement of the thicker base laminate was also suppressed. The strain energy release rate was calculated using the Eshelby energy momentum tensor for a plate. Overlapping prevention was enforced. The growth procedure was performed by moving the delamination crack front by a small increment in the outward normal direction.

In this study, the Mindlin plate finite element is used to model the response of delaminated composite plates under in-plane compression. The crack closure method is used to calculate the strain energy release rate at the delamination front. Attention is focused on 1) evaluation of the accuracy of the present method in calculating the strain energy release rate by comparing with existing three-dimensional solutions, 2) effects of stacking sequence of the laminate and shape of delamination on the strain energy release rate distribution along the delamination front, and 3) modeling the growth of delamination.

Since it is likely that the delamination will occur at an interface of two laminae with dissimilar fiber orientations, the total strain energy release rate is chosen as the fracture criterion. It has been documented that the mode I and mode II components of the fracture toughness for tough resins may be nearly equal allowing the use of the total strain energy release rate as the fracture criterion.[16] For brittle resin systems, mode separation is necessary.

Received Feb. 13, 1995; revision received July 5, 1995; accepted for publication July 16, 1995.

*Graduate Student, Department of Aeronautics and Astronautics.
†Research Associate, School of Aeronautics and Astronautics; currently at Everready Battery, 25225 Detroit Road, P.O. Box 450777, Westlake, OH 44145.
‡Professor, School of Aeronautics and Astronautics. Fellow AIAA.

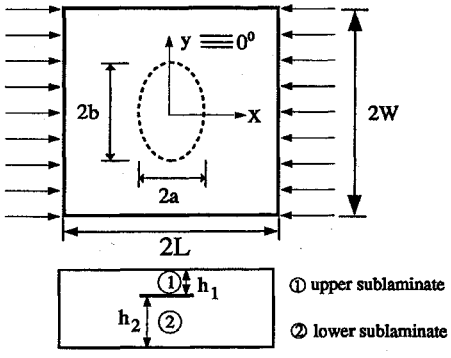

Fig. 1 Configuration of embedded delamination.

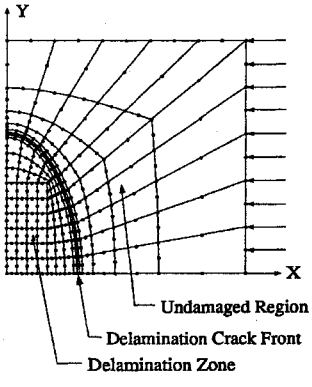

Fig. 2 Example finite element mesh.

II. Finite Element Modeling

Two finite element programs are used for the analysis. A commercial code, ABAQUS, is used to analyze stationary elliptic delaminations and to study the effects of overlapping crack surfaces. Gap elements provided by ABAQUS are used to prevent the interpenetration of the nodes of the two plates in the delamination zone. The eight-noded shell element, S8R, is chosen to model the laminated plates. The other program, FECM209, is a Fortran program developed at Purdue University for linear and nonlinear static and dynamic analysis of composite laminated plates using Mindlin plate element. It is extended to simulate the propagation of the delamination front.

Figure 1 shows a typical embedded delamination in a composite plate. The entire laminate is modeled by two plates forming an upper and lower sublaminate. The nodes are located on the midplanes of the sublaminates. An example finite element mesh is shown in Fig. 2 for a quadrant of the plate. Constraint equations are imposed on the two plates in the undelaminated region in order to enforce compatibility along the interface.

The displacement field according to the usual Mindlin plate theory is as follows:

$$\begin{aligned} u_x &= u_x^0 + z\psi_x \\ u_y &= u_y^0 + z\psi_y \\ u_z &= u_z^0 \end{aligned} \tag{1}$$

In the undelaminated region, the upper and lower sublaminates must be tied together in both displacements and rotations along the interface, i.e.,

$$\begin{aligned} u_x^0 - (h_1/2)\psi_x &= u_x^{0'} + (h_2/2)\psi_x' \\ u_y^0 - (h_1/2)\psi_y &= u_y^{0'} + (h_2/2)\psi_y' \\ u_z^0 &= u_z^{0'} \end{aligned} \tag{2}$$

The unprimed and primed quantities refer to the upper and lower sublaminates, respectively, as indicated in Fig. 1. Note that Eq. (2) requires only the displacements of the two plates along the interface to be continuous, whereas the plate rotations are not constrained.

The constraint conditions in Eq. (2) are input as linear multipoint constraints using the EQUATION command in ABAQUS. The plates are physically separated in space through enforcing displacement compatibility at the interface. The half-thickness of each plate in Eq. (2) defines the z-coordinate location in Eq. (1) of the midplane from the interface.

The loading consists of a three-step process. A small transverse perturbation load is applied at the center of the delamination of the upper sublaminate to initiate a transverse deflection. A uniform in-plane displacement is simultaneously applied along the edge of the laminate. After buckling occurs, the transverse load is removed, and the applied edge displacement is increased to obtain a desired loading level.

For the analysis in which the overlapping of the upper and lower sublaminates in the delamination zone is to be prevented, gap elements are used. These elements allow the nodes to be either in contact or separated by a specified distance. Specifically, the element GAPUNI in ABAQUS is chosen.

A. Crack Closure Method

The modified crack closure technique[17,18] is used to calculate the strain energy release rate. In this technique, the strain energy released during crack extension is assumed to be equal to the work needed to close the opened surfaces. Generally, if the relationship between the nodal force and relative displacement is nonlinear, the closure operation must be performed incrementally.[19] It was discovered, however, that even under postbuckling the relations between the nodal force (moment) and relative displacement (rotation) are nearly linear at the delamination front. Thus, one-step closure is adopted in this study.

In the crack closure method, the virtual crack extension Δa is usually taken to be small compared to the crack length. Thus, the nodal displacements (crack opening displacements) at the original crack tip after the extension can be approximated by the nodal displacements behind the crack tip before the extension. This reduces the analysis to one step instead of two. This procedure is valid if the elements in front of and directly behind the delamination crack front are similar. The conditions for similarity require that the size of each element both in front of and directly behind the crack front must be equal, the length of the elements normal to the delamination front must be Δa, and ideally the two sides of the elements should be made perpendicular to the delamination front.

Figure 3 shows a model of a pair of four elements in the upper and lower sublaminates at the delamination front. The crack front is located beneath nodes c_j ($j = 1$–5). The upper nodes c_j, d_j, and e_j are tied to the corresponding lower nodes c_j', d_j', and e_j', respectively, by the constraint conditions in Eq. (2). These constraints result in reaction forces N_x, N_y, and N_z and moments M_x and M_y at these nodes. The reaction forces and moments at a node are equal to the respective sums of the nodal forces and moments of all of the elements sharing this node.

Assume that the crack front extends from the current location c_j-c_j' to e_j-e_j'. Since the extension Δa is very small, the crack opening displacements at c_j and c_j' are taken to be the same as those at a_j and a_j' before the assumed crack extension. A similar argument is adopted for the crack opening displacements at d_j and d_j'. Thus, the

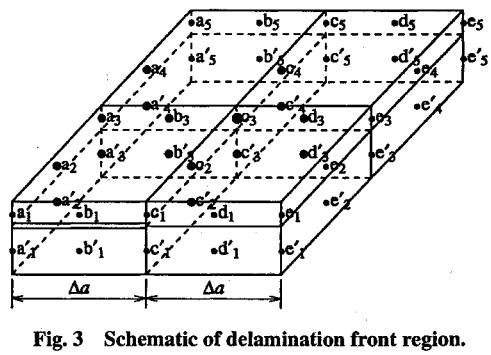

Fig. 3 Schematic of delamination front region.

crack closure energy associated with a pair of nodes (say, c_1 and c_1') can be expressed in the form

$$2U = N_x\Delta u_x + N_y\Delta u_y + N_z\Delta u_z + M_x\Delta\psi_x + M_y\Delta\psi_y + N_x'\Delta u_x' + N_y'\Delta u_y' + N_z'\Delta u_z' + M_x'\Delta\psi_x' + M_y'\Delta\psi_y' \quad (3)$$

where $N_i(M_i)$ and $N_i'(M_i')$ are nodal constraining forces (moments) before crack extension at nodes c_1 and c_1', respectively, and $u_i(\psi_i)$ and $u_i'(\psi_i')$ are the nodal displacements (rotations) at nodes a_1 and a_1', respectively. Also, Δu_i denotes the difference of the nodal displacements between nodes a_j and c_j, and $\Delta u_i'$ denotes the relative displacements between nodes a_j' and c_j'.

Using the equilibrium conditions on the constraining forces and moments together with Eq. (2), the closure energy of Eq. (3) at the pair of nodes can be written as

$$2U = N_x\left(u_x - u_x' - \frac{h_1+h_2}{2}\psi_x'\right) + N_y\left(u_y - u_y' - \frac{h_1+h_2}{2}\psi_y'\right) + N_Z(u_z - u_z') + M_x(\psi_x - \psi_x') + M_y(\psi_y - \psi_y') \quad (4)$$

The strain energy released over an area associated with the assumed crack extension can be calculated using Eq. (3) or Eq. (4) for all of the nodes in this area. The average strain energy release rate is obtained by dividing the total strain energy released by the local area. For example, the total strain energy released over the area c_2, c_4, e_4, and e_2 is calculated as

$$U = U_{c_3c_3'} + U_{d_3d_3'} + \tfrac{1}{2}\left(U_{c_2c_2'} + U_{c_4c_4'}\right) \quad (5)$$

The strain energy release rate at point c_3 is taken as

$$G = U/A \quad (6)$$

where

$$A = \Delta a \times \overline{c_2c_4} \quad (7)$$

The accuracy of such calculation obviously depends on the finite element mesh, especially at the crack front.

B. Mesh Generator

The primary purpose of the mesh generator is to translate the geometry of a delamination crack front into node locations or coordinates and to smoothly fill the mesh to the desired boundary. The most critical region of the mesh is the delamination crack front. The first objective is to arrange the nodes along the crack front so that the elements in front of and behind the crack front are similar. To achieve this similarity condition, the components of the unit normal vectors at the nodes along the front are computed. The element sides are placed as closely as possible to be parallel or perpendicular to the normal vector.

The mesh in Fig. 2 shows elements of equal size distributed along the delamination front. The generator is capable of allowing the size of the elements to be set by the user in order to obtain more accurate results for distribution of the strain energy release rate. In other words, the mesh can be refined in local regions to obtain more accurate results without adding elements. The delamination front coordinates can be generated from an equation or read from a file containing discrete coordinates and reinterpolated in order to obtain the desired element sizing or density along the front.

The interpolation is performed by a cubic spline routine. A cubic spline routine is chosen because the original coordinates read into the routine are not altered as is the case with an ordinary curve fitting routine. This is important for determining the progression of delamination using an adaptive method because the curve fitting routine is not allowed to alter a predetermined or adapted delamination shape.

The x and y coordinates of the delamination front are splined individually as a function of the arc length position s along the front. The arc length position is defined as the length of the crack front from the x axis to a respective coordinate. It was found that this method greatly reduced oscillations caused by using a sparse number of coordinates.

The remainder of the mesh is filled in according to the spacing of the nodes along the delamination front. The nodes along the rectangular boundary in the delamination zone and the outer edge boundary of the plate are positioned as a function of the spacing of the nodes along the delamination crack front. The nodes are then connected between the boundaries, and the elements are filled in appropriately according to algebraic routines.

C. Successive Delamination Growth Procedure

The program FECM209 developed at Purdue University is used to simulate delamination propagation. This program evaluates the distribution of the strain energy release rate and advances the delamination crack front at the points where the strain energy release rates exceed the critical value. The advancement is based on the difference between interlaminar toughness G_{cr} and the local value of the strain energy release rate computed along the delamination front. Specifically, the routine proceeds as follows.

1) Calculate the linear stiffness matrix.

2) Apply the in-plane load incrementally by a specified amount $\Delta\varepsilon_0$ until the final load is reached.

3) Compute the nonlinear stiffness matrix based on the current stress field and displacements.

4) Solve the displacement and stress fields.

5) Find the converged solution or return to step 3 if the solution is not convergent.

6) Evaluate the strain energy release rate along the delamination front.

7) Check the distribution of the strain energy release rate to find the corner nodes that exceed the critical value. If none exist, return to step 2.

8) Move the nodes in the outward normal direction to the delamination front where the critical strain energy release rate is exceeded and generate a new mesh.

9) Compute the linear stiffness matrix for the current mesh.

10) Go to step 3.

In step 6 the local value of G is computed by Eqs. (5–7) at every corner node. When the strain energy release rate at a node exceeds G_{cr}, the node will propagate in the local outward normal directions. The amount of propagation is proportional to the difference in the strain energy release rate and G_{cr}.

During the remeshing, the ratios of element sizes along the delamination front remain constant. Also, the number of elements along the x and y axes remains constant. A large change in element sizing could lead to poor results.

One problem with changing the mesh during loading is that the stiffness matrix must be updated accordingly. In step 9, the linear stiffness matrix is updated based on the current mesh, but the nonlinear stiffness matrix must be calculated based on current displacements and stress fields. Since the location of the nodes has changed, the displacements and stresses at the new location should be interpolated from those at the previous locations. However, since the movements of the nodes are very small each time the mesh is updated, the displacements and stresses at the previous location can be used as an approximation for the current location.

Most commonly used commercial codes do not allow the movement of nodes in a mesh during the loading procedure. Consequently, after the mesh is updated, the loading procedure would have to be restarted. In other words, the whole loading process has to be restarted for each movement of the delamination front. This is computationally very time consuming for simulating delamination growth.

III. Results and Discussion

The first objective is to verify the accuracy of the present plate model by comparing with a three-dimensional solid finite element modeled by Whitcomb.[13] Comparisons are made on the distribution of the strain energy release rate and peak transverse out-of-plane deflection for a transversely isotropic material. The subsequent work includes studying the effects of overlapping of the upper and lower sublaminates in the delamination zone on the distribution of G and

the effects of varying the shape and size of an embedded elliptic delamination on the distribution of the strain energy release rate. Finally, the growth of delamination is analyzed using the technique that progressively adapted the delamination shape as described in Sec. III.C. Both embedded and edge delaminations are considered.

A. Comparison with the Three-Dimensional Solution

Whitcomb[13] considered the case of a quasi-isotropic laminate $[\pm 45/0/90]_s$. He smeared the laminate properties by averaging the lamina properties as follows:

$$\bar{C}_{ij} = \frac{1}{8}\sum_{k=1}^{8} C_{ij}^{(k)} \tag{8}$$

where $C_{ij}^{(k)}$ are the elastic constants of the kth ply referred to the $x-y$ coordinates. This resulted in a transversely isotropic solid with the equivalent engineering material constants (in gigapascals)

$$\begin{aligned} \bar{E}_1 &= \bar{E}_2 = 52.58, \qquad \bar{E}_3 = 12.66 \\ \bar{G}_{12} &= 20.14, \qquad \bar{G}_{13} = \bar{G}_{23} = 4.48 \\ \bar{\nu}_{12} &= 0.31, \qquad \bar{\nu}_{13} = \bar{\nu}_{23} = 0.33 \end{aligned} \tag{9}$$

Comparisons are made for two circular delamination cracks with $R = 15$ and 30 mm, and an elliptic crack with $b \times a = 30 \times 15$ mm. The loading direction is parallel to the x axis. The upper and lower plate thicknesses are 0.4 and 3.6 mm, respectively. The quarter-model dimensions are $L = W = 50$ mm. Both the distribution of the strain energy release rate G and peak transverse midplane deflection at the center of the delaminated plate w_0 are compared.

Figure 4 shows the distributions of G at a loading strain level of 0.5% for the two circular delamination cracks and the elliptical crack. Overlapping of the crack surfaces is allowed in the three-dimensional and double plate solutions. The open circles on the plots indicate the region where overlapping occurs. Figure 5 shows the maximum transverse deflection w_0 of the upper plate for each of the three delamination shapes. It is evident that the present plate solutions agree very well with Whitcomb's three-dimensional solutions in deflection as well as strain energy release rate.

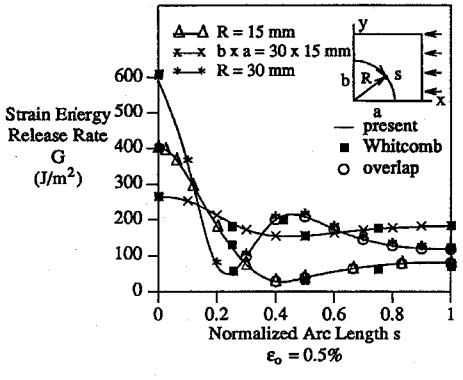

Fig. 4 Strain energy release rate distribution comparisons.

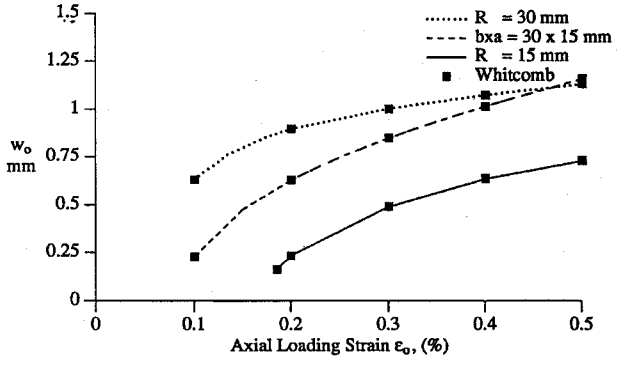

Fig. 5 Peak transverse deflection of the upper sublaminate.

Table 1 Error caused by overlapping

Ellipse aspect ratio	Percent error in maximum strain energy release rate, Strain levels, %[a]				
	0.20	0.30	0.40	0.50	0.60
0.5	[b]	[b]	[b]	[b]	−678
0.8	[b]	−7.62	−4.21	1.89	8.04
1	−0.22	−0.74	0.39	3.06	6.46
1.5	0.04	−0.06	−0.07	0.11	0.39
2	0.00 (a,0)	0.00 (a,0)	0.00	0.00	0.00
2.5	0.10 (a,0)	3.41 (a,0)	3.65 (a,0)	2.13 (a,0)	−0.06[c]

[a]Maximum value is at the point $(0, b)$ unless otherwise labeled.
[b]Strain level is below the buckling load.
[c]Maximum is at a point near $(0, b)$.

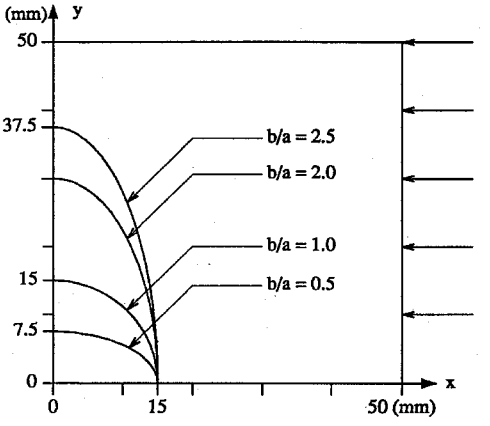

Fig. 6 Ideal elliptical delamination cracks; a quadrant shown.

B. Effects of Overlapping

The effect of allowing the upper and lower sublaminates to interpenetrate on the strain energy release rate is studied. A range of ellipse aspect ratios $b/a = 0.5-2.5$ as shown in Fig. 6 is considered. The elliptical delaminations are generated by holding the x-axis length constant. The analyses are performed using ABAQUS. Solutions enforcing a contact condition using the gap element are also obtained for comparison.

Table 1 shows the error due to overlapping on the maximum value of the strain energy release rate for a range of loading levels using the properties from Eq. (9). The maximum value of the strain energy release rate is at the point $(0, b)$ for smaller ellipse aspect ratios and shifts to the point $(a, 0)$ for larger aspect ratios. Overlapping occurs in the region of the delamination zone near the point $(a, 0)$.

In general, it is found that overlapping increases for decreasing ellipse aspect ratios and with increasing strain levels.[20] For delaminations with small aspect ratios, a very large overlapping region along the x axis may occur. For such cases, the strain energy release rate distribution can be significantly affected inside and outside this region.

C. Effect of Stacking Sequence

The effect of stacking sequence on the strain energy release rate is also studied. The stacking sequences for the embedded delamination are $[(90/0)_s//90_{14}/0_{14}]$, $[(0/90)_s//90_{14}/0_{14}]$, $[(90_2/0_2)//90_{14}/0_{14}]$, and $[(90/0)_2//90_{14}/0_{14}]$. The double slash indicates the location of delamination interface. The 0-deg direction is parallel to the loading direction. These laminates are referred to by the upper sublaminate stacking sequence as $[(90/0)_s]$, $[(0/90)_s]$, $[90_2/0_2]$, and $[(90/0)_2]$, respectively. Note that the upper sublaminates all consist of four plies.

The ply thickness is 0.127 mm. Thus, the thicknesses of the upper (h_1) and lower (h_2) sublaminates are 0.508 and 3.556 mm, respectively. The elastic constants (in gigapascals) for the composite are given by

$$\begin{aligned} E_1 &= 143, \qquad E_2 = E_3 = 10.2 \\ G_{12} &= G_{13} = 5.52, \qquad G_{23} = 3.43 \\ \nu_{12} &= \nu_{13} = 0.3, \qquad \nu_{32} = 0.49 \end{aligned} \tag{10}$$

The stiffnesses of these sublaminates are obtained according to the lamination theory[21] as follows.

Extensional stiffness matrix for all stacking sequences (in newtons per meter):

$$[A] = \begin{bmatrix} 0.392 & 0.0156 & 0 \\ 0.0156 & 0.392 & 0 \\ 0 & 0 & 0.0280 \end{bmatrix} \times 10^8$$

Bending stiffness for symmetric laminates (in newton meters):

$$[D]_{[(90/0)_s]} = \begin{bmatrix} 0.295 & 0.0336 & 0 \\ 0.0336 & 1.39 & 0 \\ 0 & 0 & 0.0603 \end{bmatrix}$$

$$[D]_{[(0/90)_s]} = \begin{bmatrix} 1.39 & 0.0336 & 0 \\ 0.0336 & 0.295 & 0 \\ 0 & 0 & 0.0603 \end{bmatrix}$$

Bending stiffness for unsymmetric laminates (in newton meters):

$$[D] = \begin{bmatrix} 0.842 & 0.0336 & 0 \\ 0.0336 & 0.842 & 0 \\ 0 & 0 & 0.0603 \end{bmatrix}$$

Bending–extension coupling stiffness (in newtons)

$$[B]_{[(90/0)_2]} = \begin{bmatrix} 0.216 & 0 & 0 \\ 0 & -0.216 & 0 \\ 0 & 0 & 0 \end{bmatrix} \times 10^4$$

$$[B]_{[(90_2/0_2)]} = \begin{bmatrix} 0.431 & 0 & 0 \\ 0 & -0.431 & 0 \\ 0 & 0 & 0 \end{bmatrix} \times 10^4$$

The analyses are performed using ABAQUS with gap elements to prevent overlapping of crack surfaces. The deflection of the lower sublaminates is suppressed to avoid global buckling.

Figures 7 and 8 present the results for the $[(90/0)_s]$ and $[(0/90)_s]$ laminates. Two embedded elliptical delaminations with aspect ratios 0.5 and 2.5, respectively, are considered. The results indicate that the strain energy release rate distribution is quite localized with the maximum value occurring at the point $(0, b)$. This implies that for both laminates the delamination growth would initiate from this point. For the delamination with aspect ratio 2.5, however, the trend is quite different, i.e., the maximum strain energy release rate for the $[(0/90)_s]$ laminate now occurs at the point $(a, 0)$.

The results of Figs. 7 and 8 also indicate that for a given loading strain, the maximum strain energy release rate in the $[(90/0)_s]$ laminate is much higher than that in the $[(0/90)_s]$ laminate. Thus, it would be easier to produce delamination growth in the $[(90/0)_s]$ laminate. It is interesting to compare this behavior to the fact that the bending stiffness D_{11} in the loading (x) direction of the $[(0/90)_s]$ laminate is much greater than that of the $[(90/0)_s]$ laminate.

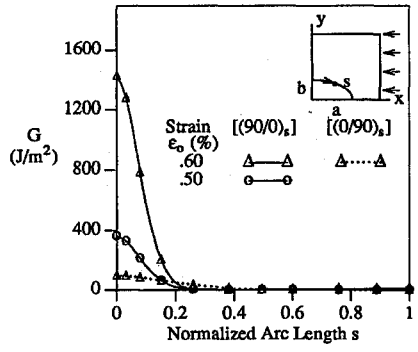

Fig. 7 Distribution of strain energy release rate for symmetric layups with ellipse aspect ratio 0.5; a = 15.0 mm and b = 7.5 mm.

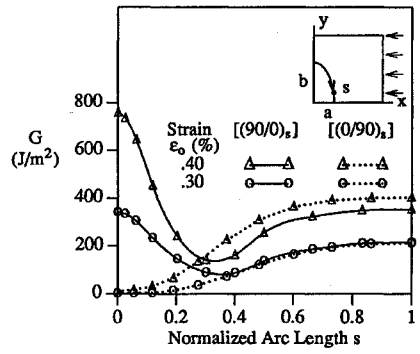

Fig. 8 Distribution of strain energy release rate for symmetric layups with ellipse aspect ratio 2.5; a = 15.0 mm and b = 37.5 mm.

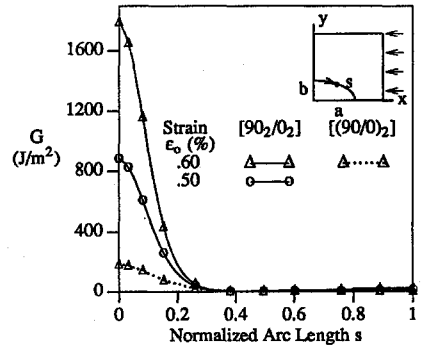

Fig. 9 Distribution of strain energy release rate for unsymmetric layups with ellipse aspect ratio 0.5; a = 15.0 mm and b = 7.5 mm.

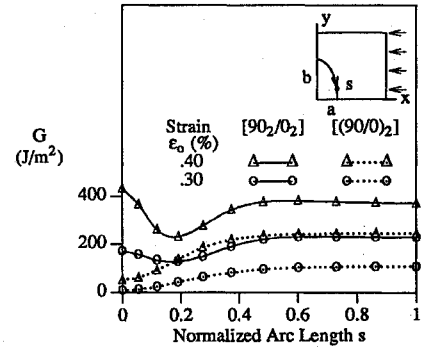

Fig. 10 Distribution of strain energy release rate for unsymmetric layups with ellipse aspect ratio 2.5; a = 15.0 mm and b = 37.5 mm.

Similar results for the $[90_2/0_2]$ and $[(90/0)_2]$ asymmetric laminates are shown in Figs. 9 and 10. These two sublaminates have identical extensional and bending stiffnesses. The $[90_2/0_2]$ laminate has a stronger extension–bending coupling, which has the effect of reducing the apparent bending stiffness of the laminate. This explains why the $[90_2/0_2]$ laminate has a higher strain energy release rate than the $[(90/0)_2]$ laminate.

D. Progressive Delamination Growth

Transversely Isotropic Plate

The transversely isotropic plate containing an embedded delamination as discussed in Sec. III.A is first considered. The growth is simulated from an initially circular delamination front with a radius of 15 mm. The critical strain energy release rate $G_{cr} = 150$ J/m^2 is chosen for the analysis. The out-of-plane deformation is constrained in the lower sublaminate. Overlapping of the sublaminates is not constrained due to the small error in both the distribution and maximum value of the strain energy release rate for the initial delamination shape and loading level considered. In fact, the delamination growth is predicted to initiate at a strain level of 0.35%, and the error due to overlapping is in the −0.74—0.39% range as seen from Table 1. Thus, preventing overlapping would be unnecessary.

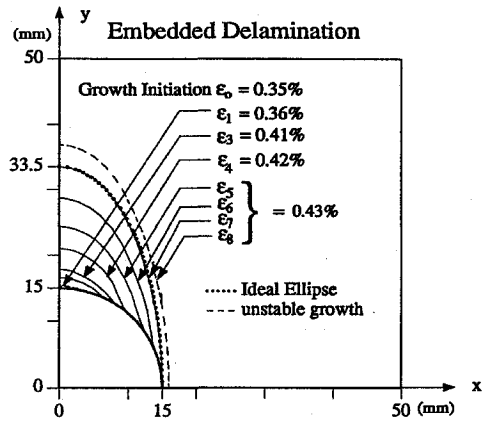

Fig. 11 Progressive delamination fronts for transversely isotropic material.

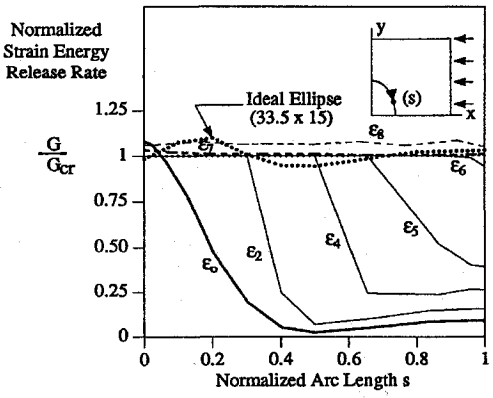

Fig. 12 Strain energy release rate distributions for transversely isotropic material.

The progressive delamination growth contours and corresponding normalized strain energy release rate distributions are shown in Figs. 11 and 12. Figure 11 shows that the loading level increases for the first five growth contours (ε_1, ε_2, ε_3, ε_4, and ε_5). Thus, the propagation is stable. The next two contours (ε_6 and ε_7) are neutrally stable since the loading level is not increased and the distribution of the strain energy release rate in the growth region remains near G_{cr}. Curve ε_7 is the growth curve before the entire delamination front starts to propagate. The last growth curve ε_8 is unstable because the distribution of the strain energy release rate has increased to about 160 J/m^2 while the loading strain level remained constant.

In Fig. 12, the distributions of the strain energy release rate for growth curves ε_2–ε_6 are set to G_{cr} in the region where growth occurred. The actual distribution has small oscillations (less than 5%) slightly below G_{cr} in the region. The dashed curves for ε_7 and ε_8 are the actual distributions. It is apparent that the distributions for ε_7 and ε_8 are nearly straight with small oscillations about G_{cr} and G = 160 J/m^2, respectively.

The dotted line in Fig. 11 represents the shape of an ideal ellipse with the same major and minor axis lengths as the ε_7 growth curve generated by the program. It is evident that these delamination growth contours appear to be elliptical. In Fig. 12, the distribution of the strain energy release rate for the ideal ellipse is shown. Although the distribution for the ideal ellipse has much larger oscillations about G_{cr} than the growth curve ε_7, the shape is very similar to the growth contour. This sensitivity makes the determination of the growth contour computationally efficient because it is not necessary to iterate the delamination front until the strain energy release rate reaches the constant value of G_{cr}.

Cross-Ply Laminates

The delamination growth of two laminates, $[(0/90)_s]$ and $[(90/0)_s]$, is simulated from an initially circular delamination front with a radius of 15 mm. A value of the critical strain energy release rate G_{cr} = 200 J/m^2 is chosen for the analysis.

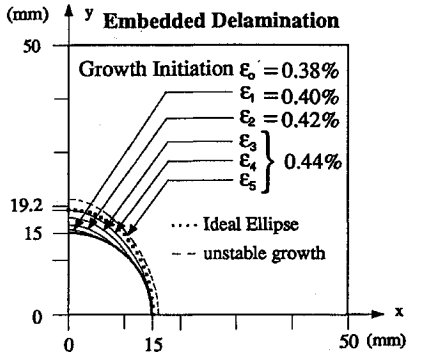

Fig. 13 Progressive delamination fronts for the $[(0/90)_s]$ laminate.

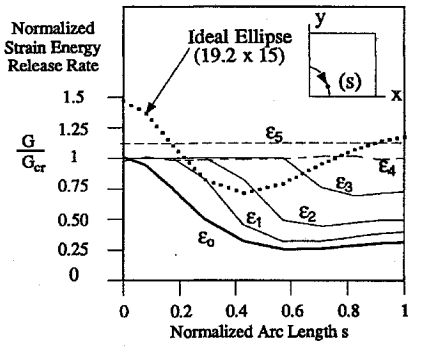

Fig. 14 Strain energy release rate distributions for the $[(0/90)_s]$ laminate.

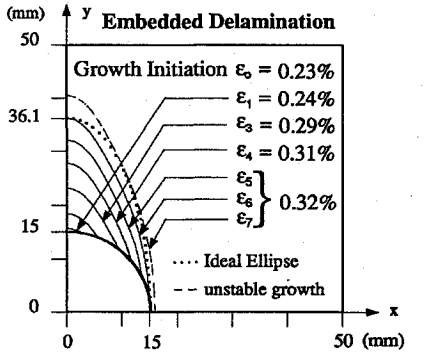

Fig. 15 Progressive delamination fronts for the $[(90/0)_s]$ laminate.

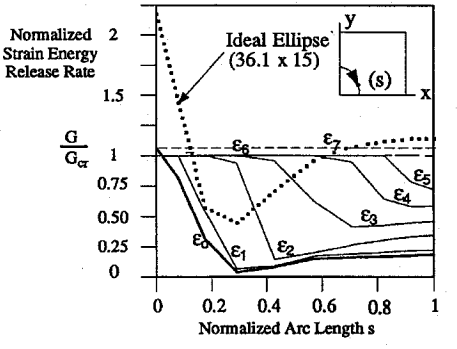

Fig. 16 Strain energy release rate distributions for the $[(90/0)_s]$ laminate.

The growth contours and corresponding strain energy release rate distributions for the $[(0/90)_s]$ laminate are shown in Figs. 13 and 14, respectively. From the increasing load level in Fig. 13, the propagation appears to be stable for the first three contours. The growth for the next contour ε_4 is neutrally stable. The curve labeled ε_5 is unstable because the strain energy release rate has increased to 220 J/m^2 while the loading level (ε_5 = 0.44%) remained constant.

The growth contours and corresponding strain energy release rate distributions for the $[(90/0)_s]$ sublaminate are shown in Figs. 15 and 16, respectively. The growth is stable for the first four loading

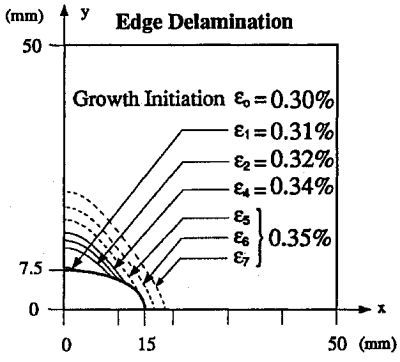

Fig. 17 Progressive delamination fronts for the $[90_2/0_2//0_2(90_4/0_4)_3/90_2]$ laminate.

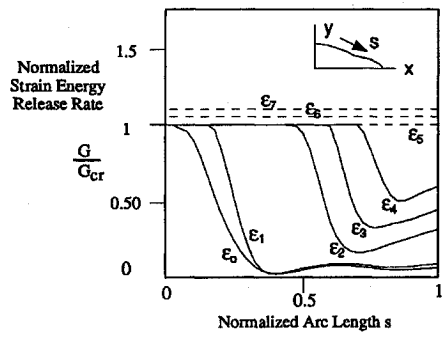

Fig. 18 Strain energy release rate distributions for the $[90_2/0_2//0_2(90_4/0_4)_3/90_2]$ laminate.

levels ($\varepsilon_1 - \varepsilon_4$) and becomes nearly neutrally stable for the curves labeled ε_5 and ε_6. The last curve labeled ε_7 is unstable because G has increased to 208 J/m^2 while the loading level remained constant. The distribution plot of G for the ideal ellipse (with the aspect ratio of contour ε_6) has a very large oscillation about the G_{cr} line. In fact, the maximum value is more than twice the value of G_{cr}. Thus, the propagating delamination cannot be modeled as an elliptical crack.

In comparing the delamination growth in the two laminates, we can see that the growth initiation load level is much lower for the $[(90/0)_s]$ laminate. The amount of stable growth is much larger for this laminate as well.

Edge Delamination

A half-elliptical edge delamination is investigated with dimensions $b = 7.5$ mm and $a = 15$ mm for a panel with a layup $[90_2/0_2//0_2(90_4/0_4)_3 90_2]$ that is subjected to in-plane compression. The material constants given by Eq. (10) are used. The critical strain energy release rate is also chosen to be 200 J/m^2. Figures 17 and 18 show the growth contours and strain energy release rate distributions, respectively. Initially, the delamination appears to grow in the direction perpendicular to the loading. The delamination growth is stable at the early stages. The delamination front appears to be triangular in shape. At a certain loading level ($\varepsilon_0 = 0.35\%$) the delamination growth becomes unstable. At this strain level, the strain energy release rate becomes larger as the delamination front propagates. The dashed lines are used to indicate the unstable delamination fronts. Along these dashed contour lines, the strain energy release rate is constant, but its magnitude increases as the delamination region increases.

IV. Conclusions

A double plate model is used to calculate the strain energy release rate along the delamination front in laminated composite plates. It is shown that the present method is highly efficient and accurate. The distribution of the strain energy release rate calculated using the present method is very sensitive to the configuration of the delamination front. This makes an accurate prediction of the delamination front computationally efficient.

The bending stiffness of the sublaminate in the delamination zone governs delamination growth. A lower bending stiffness in the loading direction would produce a greater strain energy release rate and thus delamination growth at the delamination front.

Acknowledgments

This work was supported by NASA Langley Research Center Grant NAG-1-1323 to Purdue University. Jerry Housner and John Wang were technical monitors.

References

[1]Chai, H., Babcock, C. A., and Knauss, W. G., "One Dimensional Modeling of Failure in Laminated Plates by Delamination Buckling," *International Journal of Solids and Structures*, Vol. 17, No. 11, 1981, pp. 1069–1083.

[2]Whitcomb, J. D., "Finite Element Analysis of Instability Related Delamination Growth," *Journal of Composite Materials*, Vol. 15, No. 9, 1981, pp. 403–426.

[3]Yin, W. L., and Wang, J. T. S., "The Energy-Release Rate in the Growth of a One-Dimensional Delamination," *Journal of Applied Mechanics*, Vol. 51, No. 4, 1984, pp. 939–941.

[4]Yin, W. L., and Jane, K. C., "Refined Buckling and Postbuckling Analysis of Two-Dimensional Delaminations—I. Analysis and Validation," *International Journal of Solids and Structures*, Vol. 29, No. 5, 1992, pp. 591–610.

[5]Yin, W. L., and Jane, K. C., "Refined Buckling and Postbuckling Analysis of Two-Dimensional Delaminations—II. Results for Anisotropic Laminates and Conclusion," *International Journal of Solids and Structures*, Vol. 29, No. 5, 1992, pp. 611–639.

[6]Chai, H., and Babcock, C. D., "Two-Dimensional Modeling of Compressive Failure in Delaminated Laminates," *Journal of Composite Materials*, Vol. 19, No. 1, 1985, pp. 67–98.

[7]Chai, H., "Buckling and Post-Buckling Behavior of Elliptical Plates: Part I Analysis," *Journal of Applied Mechanics*, Vol. 57, No. 4, 1990, pp. 981–988.

[8]Chai, H., "Buckling and Post-Buckling Behavior of Elliptical Plates: Part II Results," *Journal of Applied Mechanics*, Vol. 57, No. 4, 1990, pp. 989–995.

[9]Whitcomb, J. D., "Instability-Related Delamination Growth of Embedded and Edge Delaminations," *Journal of Composites Technology and Research*, Vol. 13, No. 3, 1991, pp. 175–178.

[10]Whitcomb, J. D., "Analysis of a Laminate with a Postbuckled Embedded Delamination, Including Contact Effects," *Journal of Composite Materials*, Vol. 26, No. 10, 1992, pp. 1523–1535.

[11]Whitcomb, J. D., "Comparison of Full 3-D, Thin-Film 3-D, and Thin-Film Plate Analyses of a Postbuckled Embedded Delamination," *Journal of Composite Technology and Research*, Vol. 11, No. 4, 1989, pp. 154–157.

[12]Whitcomb, J. D., "Predicted and Observed Effects of Stacking Sequence and Delamination Size on Instability Related Delamination Growth," *Journal of Composites Technology and Research*, Vol. 11, No. 3, 1989, pp. 94–98.

[13]Whitcomb, J. D., "Three-Dimensional Analysis of a Postbuckled Embedded Delamination," *Journal of Composite Materials*, Vol. 23, No. 9, 1989, pp. 862–889.

[14]Nilsson, K.-F., and Giannakopoulos, A. E., "Finite Element Simulation of Delamination Growth," *Proceedings of the First International Conference on Computer-Aided Assessment and Control of Localized Damage* (Portsmith, UK), edited by H. Aliabadi, A. Brebbia, and D. J. Cartwright, Springer, Berlin, 1990, pp. 299–313.

[15]Nilsson, K.-F., Thesken, J. C., Sindelar, P., Giannakopoulos, A. E., and Storakers, B., "A Theoretical and Experimental Investigation of Buckling Induced Delamination Growth," *Journal of the Mechanics and Physics of Solids*, Vol. 41, No. 4, 1993, pp. 749–782.

[16]Johnson, W. S., and Mangalgiri, P. D., "Influence of the Resin on Interlaminar Mixed-Mode Fracture," *Toughened Composites*, edited by N. J. Johnston, American Society for Testing Materials, Philadelphia, 1987, pp. 295–315 (ASTM STP 937).

[17]Ribyki, E. F., and Kannien, M. F., "A Finite Element Calculation of Stress Intensity Factors by a Modified Crack Closure Integral," *Engineering Fracture Mechanics*, Vol. 9, No. 4, 1977, pp. 931–938.

[18]Jih, C. J., and Sun, C. T., "Evaluation of a Finite Element Based Crack-Closure Method for Calculating Static and Dynamic Energy Release Rates," *Engineering Fracture Mechanics*, Vol. 37, No. 2, 1990, pp. 313–322.

[19]Cheong, S. K., and Sun, C. T., "Analysis of Postbuckled Delaminations Using Incremental Crack Closure Integral," *Proceedings of the Second International Symposium on Composite Structures and Materials*, Peking Press, Beijing, PRC, 1992, pp. 519–524.

[20]Klug, J., "Efficient Modeling of Postbuckling Delamination Growth in Composite Laminates Using Plate Elements," M.S. Thesis, School of Aeronautics and Astronautics, Purdue Univ., West Lafayette, IN, 1994.

[21]Jones, R., *Mechanics of Composite Materials*, Scripta, Washington, DC, 1975, Chap. 4.